Eur. Phys. J. E **23**, 247–254 (2007)
DOI 10.1140/epje/i2007-10202-8

THE EUROPEAN PHYSICAL JOURNAL E

Influence of cholesterol on the bilayer properties of monounsaturated phosphatidylcholine unilamellar vesicles

N. Kučerka[1,2,a], J. Pencer[1], M.-P. Nieh[1], and J. Katsaras[1,3,4,b]

[1] Canadian Neutron Beam Centre, National Research Council, Chalk River, Ontario K0J 1P0, Canada
[2] Department of Physical Chemistry of Drugs, Faculty of Pharmacy, Comenius University, 832 32 Bratislava, Slovakia
[3] Guelph-Waterloo Physics Institute and Biophysics Interdepartmental Group, University of Guelph, Guelph, Ontario N1G 2W1, Canada
[4] Department of Physics, Brock University, 500 Glenridge Avenue, St. Catharines, Ontario L2S 3A1, Canada

Received 19 March 2007
Published online: 5 July 2007 –

Abstract. The influence of cholesterol on the structure of unilamellar-vesicle (ULV) phospholipid bilayers is studied using small-angle neutron scattering. ULVs made up of short-, mid- and long-chain monounsaturated phospholipids (diC_n:1PC, $n = 14$, 18, 22, respectively) are examined over a range (0–45 mol %) of cholesterol concentrations. Cholesterol's effect on bilayer structure is characterized through changes to the lipid's transmembrane thickness, lateral area and headgroup hydration. For all three lipids, analysis of the experimental data shows that the addition of cholesterol results in a monotonic increase of these parameters. In the case of the short- and mid-chain lipids, this is an expected result, however, such a finding was unexpected for the long-chain lipid. This implies that cholesterol has a pronounced effect on the lipid's hydrocarbon chain organization.

PACS. 61.12.Ex Neutron scattering (including small-angle scattering) – 87.14.Cc Lipids – 87.16.Dg Membranes, bilayers, and vesicles – 87.68.+z Biomaterials and biological interfaces

1 Introduction

Cholesterol, a ubiquitous component of mammalian cell membranes, plays an important role as a signaling molecule [1], a modulator of lateral membrane organization [2], and influences the membrane's material properties *e.g.*, "fluidity" [3] and bending rigidity [4]. Furthermore, cholesterol levels in both cell and model membranes have been found to modulate the activity of certain transmembrane proteins [5–8]. Nevertheless, despite its importance, a comprehensive understanding of cholesterol-lipid interactions has yet to be achieved.

It has been noted that the addition of cholesterol to fluid phase lipid bilayers results in increased acyl chain order [9–13], while having the opposite effect on lipid headgroups. The consensus of a number of studies, including NMR [14,15], EPR [16,17] and fluorescence [18], is that cholesterol acts as a "spacer" molecule, increasing the separation between lipid headgroups, thereby reducing possible interactions between them. These studies further demonstrate that, while the addition of cholesterol decreases the extent of water penetration into the membrane's hydrophobic region, there is a concomitant increase in headgroup hydration.

It is generally accepted that the function of membrane proteins depends on the membrane's state and lipid composition [7,19]. Previously, there has been some conjecture that the ability of cholesterol to modulate protein activity could in part be due to the influence of cholesterol on membrane thickness —controlling the hydrophobic mismatch between the protein's transmembrane segments and the bilayer's hydrophobic region [5]. The reported influence of cholesterol on bilayer thickness suggests a dependence on the length of the lipid's acyl chains, their saturation level and bilayer hydration [20–23]. Nevertheless, while cholesterol contributes to increasing the thickness of fully hydrated bilayers made up of saturated lipids (*i.e.* up to 18 carbons long [20]), its effect on unsaturated lipids, as observed by small-angle X-ray diffraction (SAXD) and/or small-angle neutron scattering (SANS), is by no means a foregone conclusion [22].

Reasons for the discrepancy between results in the literature are not clear, but could arise from a number of factors such as: a) Compared to saturated lipids, cholesterol at high concentrations may tend to poorly solubilize in unsaturated lipid membranes [24–27]. b) The lateral

[a] e-mail: Norbert.Kucerka@nrc.gc.ca
[b] e-mail: John.Katsaras@nrc.gc.ca

distribution of cholesterol in the membrane may be non-uniform and may lead to domain formation [23,26]. c) Increased headgroup hydration [12,15–18] may result in an apparent thinning of the membrane at elevated concentrations of cholesterol. d) Differences in sensitivity between SAXD and SANS may lead to different assessments of membrane structural parameters, as disparate results, even for pure lipid bilayers, have been reported in the literature [28].

Here, we report measurements on unilamellar vesicles (ULVs) made from differing chain length (*i.e.* 14, 18 and 22 carbons) monounsaturated phospholipids, as a function of cholesterol content. SANS is used to determine cholesterol's influence on bilayer structure, as was previously done by Gallová, *et al.* [21,22]. However, here we extend these measurements to include a range of cholesterol concentrations, not previously examined. The incorporation of cholesterol, for all concentrations, was inferred from fluorescence anisotropy measurements.

Bilayer structure is determined from SANS using a model described by Kučerka *et al.* [29] that includes, compared to commonly used single-strip models, a more detailed description of the bilayer. This model allows us to extract accurate structural parameters and explicitly identifies the amount of water present in the bilayer. Cholesterol's effect on the lipid bilayer is characterized through the changes to the membrane's thickness, lateral area and hydration. diC18:1PC's cholesterol dependence is determined at 0, 17, 29, 38 and 45 mol % cholesterol content. The measured trends from diC18:1PC bilayers are then applied to the two other systems (*i.e.* diC14:1PC and diC22:1PC) which contain 0 and 40 mol % cholesterol. Interestingly, we find that cholesterol affects, in a similar fashion, the structural parameters of the three systems studied.

2 Materials and methods

Synthetic 1,2-dioleoyl-*sn*-glycero-3-phosphorylcholine (diC18:1PC), 1,2-dimyristoleoyl-*sn*-glycero-3- phosphorylcholine (diC14:1PC) and 1,2-dierucoyl-*sn*-glycero-3-phosphorylcholine (diC22:1PC) were purchased from Avanti Polar Lipids, Inc. (Birmingham, AL) and used without further purification. Cholesterol was obtained from Sigma-Aldrich (St. Louis, MO). All other chemicals were reagent grade.

Lipids were co-solubilized in chloroform with an appropriate amount of cholesterol in a glass vial. The chloroform was then evaporated under a stream of nitrogen gas followed by vacuum pumping. The lipid film was then dispersed in D_2O at a total lipid concentration ranging from 10 to 20 mg/ml. The lipid dispersions were extruded using either a pneumatic (LiposoFast^{TM}, Avestin, Inc., Ottawa) or hand-held extruder (Avanti Polar Lipids, Inc.). Vesicles were extruded using polycarbonate filters with pore diameters of 2000 Å (9 times), 1000 Å (9 times) and 500 Å (19 times), or two filters with pore diameters of 500 Å (25 times); hence the final ULV size ~ 600 Å [30].

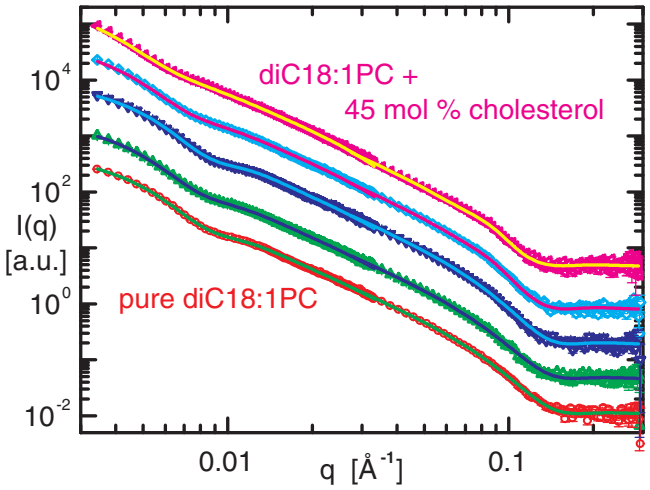

Fig. 1. (Color online) Experimental SANS data obtained from ULVs dispersed in D_2O. Scattering curves are shifted vertically for clarity of presentation. From bottom to top, they correspond to diC18:1PC bilayers containing 0, 17, 29, 38, and 45 mol % of cholesterol. Solid lines represent the best fits to the data.

Fluorescence anisotropy measurements were perfomed with a Fluorolog FL3-22 fluorimeter (Instruments S.A., Inc.) using excitation and emission wavelengths of 366 nm and 427 nm, respectively. It has been demonstrated recently [31,32], that the fluorescence anisotropy of lipid bilayers changes with lipid order parameters, and so it is a direct indicative of membrane order.

SANS measurements were carried out at the 30 m NG3 and NG7 SANS instruments [33] located at the National Institute of Standards and Technology (Gaithersburg, MD). 1.5 and 12 m sample-to-detector distances (SDD) were used along with a neutron wavelength, λ, of 8 Å ($\delta\lambda/\lambda = 10\%$), and 4 and 1 m SDD along with $\lambda = 5.5$ Å ($\delta\lambda/\lambda = 10\%$), resulting in a total range in scattering vector ($q = 4\pi \sin(\theta/2)/\lambda$, where θ is a scattering angle) of $0.003 < q < 0.3$ Å^{-1}. Data were collected using a 640 mm × 640 mm 2D ^{3}He position-sensitive detector with 5 mm × 5 mm resolution. Samples were contained in standard, 2-mm-path-length quartz cells. Acquired images were corrected using a suite of software supplied by NIST [34]. Representative, corrected one-dimensional (1-D) scattering curves are shown in Figure 1 together with the best fits to the data.

2.1 Data analysis

The experimentally measured scattering intensity for a polydisperse system of spherical vesicles has the form

$$I(q) = \int_R G(R) \left[4\pi \int_{R-d/2}^{R+d/2} r^2 \rho(r) \frac{\sin(qr)}{qr} \mathrm{d}r \right]^2 \mathrm{d}R, \quad (1)$$

where $\rho(r)$ is the scattering length density (SLD) as a function of radial distance from the center of the ULV and

d is the bilayer thickness. The size distribution function, $G(R)$ can be represented by the Schulz distribution

$$G(R) = \left(\frac{z+1}{R_m}\right)^{z+1} \frac{R^z}{\Gamma(z+1)} \exp\left[\frac{-R(z+1)}{R_m}\right], \quad (2)$$

where R_m is the mean radius (distance from the vesicle center to the bilayer midplane) and the variance is $\sigma^2 = R_m^2/(z+1)$.

Following Pencer *et al.* [35], we can separate the parts corresponding to the symmetric bilayer and vesicle. The scattered intensity is then calculated as the square of the planar bilayer form factor and multiplied by the function which includes the particle's "sphericity" and the system's polydispersity, $P_{TS}(q)$, and is written as follows:

$$I(q) = P_{TS}(q)F^2(q) \quad (3)$$

$$P_{TS}(q) = \frac{8\pi^2(z+1)(z+2)}{s^2q^2}\left\{1 - \left(1+\frac{4q^2}{s^2}\right)^{-(z+3)/2} \times \cos\left[(z+3)\arctan\left(\frac{2q}{s}\right)\right]\right\},$$

where $s = R_m/\sigma_R^2$ and $z = R_m^2/\sigma_R^2 - 1$ are the products of the vesicle mean radius R_m and σ_R represents the system's polydispersity. The bilayer form factor $F(q)$ is the well-known Fourier transform for a symmetric SLD profile, and is written as

$$F(q) = 2\int_0^{d/2} [\rho(r) - \rho_W]\cos(qr)\mathrm{d}r, \quad (4)$$

where ρ_W is the SLD of water. The bilayer's SLD profile, $\rho(r)$, is a sum of the SLD weighted probabilities of all the subgroups (W: water, H: headgroup, C: hydrocarbon)

$$\rho(r) = \sum_{i=W,H,C} \rho_i P_i(r). \quad (5)$$

The probability distributions $P_i(r)$ will be defined in the next section.

2.2 Structural model

Most analysis of small-angle neutron scattering data has either been based on the Kratky-Porod approximation, or by fitting the data to a simple single-strip model of the bilayer [21,22,36–38]. Although this approach is rather popular, it neglects the inner structural details of the bilayer. The obtained structural values, therefore, may not be an accurate measure of the bilayer's molecular organization.

Recently, there has been progress in the use of more accurate models to analyze SANS data [29,39]. These models were inspired by the results from molecular-dynamics simulations, which show additional substructure within the bilayer. Of particular importance in this development was the replacement of a sharp water-bilayer interface by a "smooth" one. This function consists of a linear term, for the distribution of water penetrating the headgroup region, and a linear term (twice the slope and opposite in sign) assigned to the part of hydrocarbon region that is found within the half width of the headgroup region (see Fig. 2). The remaining part of this region is then completed by the triangular shape of headgroup itself while the central hydrocarbon region is modeled by a simple constant. This construction satisfies the complementarity rule, which states that the total probability is equal to unity across the entire bilayer (see Eq. (6)).

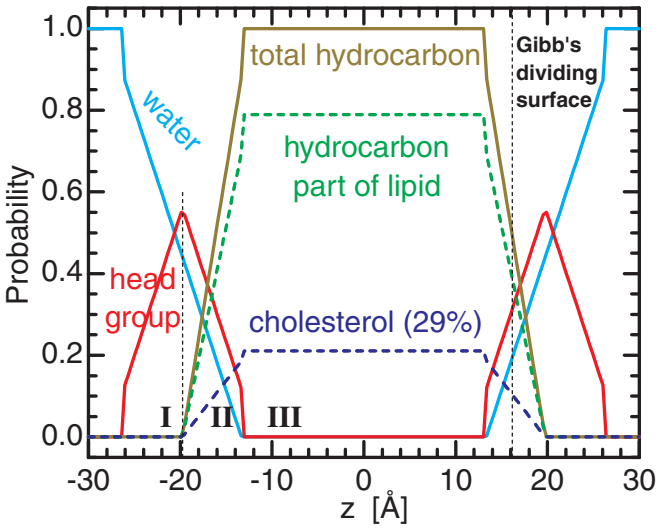

Fig. 2. (Color online) Probability distributions of the bilayer subgroups shown for diC18:1PC containing 29 mol % cholesterol. The water, headgroup, and hydrocarbon regions are shown explicitly (solid lines). Broken lines show the partitioning probability contributions for the lipid and cholesterol in the hydrocarbon region.

The mathematical description of this model's probability distributions (*i.e.* water, headgroup, hydrocarbon) for the three different bilayer regions (*i.e.* I: outer half of the headgroup region, II: inner half of the headgroup region, III: hydrocarbon region) is given as

region	water	headgroup	hydrocarbon
I	$-kr + c_2$	$+kr + (1 - c_2)$	$+0$
II	$-kr + c_2$	$-kr + (1 - c_2 - c_1)$	$+2kr + c_1$
III	0	$+1$	$+0$

(6)

where the slope k is calculated from the volume of the headgroup (V_H) and water (V_W), and the lipid area (A_L)

$$k = \frac{2A_L N'_W V_W}{(V_H + N'_W V_W)^2}, \quad (7)$$

and N'_W is the number of water molecules in the headgroup region. The constants c_1 and c_2 are calculated from the probability values at $r_2 = V_C/A_L$ (interface between the hydrocarbon (III) and headgroup (II) regions) and at $r_1 = (V_C + (V_H + N'_W V_W)/2)/A_L$ (maximum of headgroup probability) as follows:

$$c_1 = -2kr_1, \quad c_2 = kr_2. \quad (8)$$

Table 1. Volumetric values (V [Å^3]) used in the analysis of the data. Values are based on published results [40–42].

CH	CH_2	CH_3	headgroup	cholesterol	water
22.3	27.7	53.5	331	633	30

The two fitting parameters, A_L and N'_W, are related through volumetric information (Tab. 1) and the headgroup thickness d_H (constrained to 10 ± 0.2 Å). The lipid area is given by

$$A_L = \frac{V_H + N'_W V_W}{d_H} = \frac{V_C}{d_C}, \qquad (9)$$

where d_C ($= d_{TOT}/2 - d_H$; d_{TOT} is the total bilayer thickness) is defined according to Gibb's dividing surface for the interface between the hydrocarbon and headgroup regions (see Fig. 2). The dividing surface criterion is that the integrated probability of the fraction of hydrocarbon molecules outside d_C is equal to the integrated deficit probability inside d_C [28]. Note that this thickness is not equal to the thickness of region III, as there are hydrocarbon molecules also present in region II.

Here, we employ a model consisting of three distinct strips, which correspond to the polar headgroup (one on each side of the bilayer) and central hydrocarbon regions ("3T" model of [29]). In the case of pure lipid bilayers an additional strip can be added for the terminal methyl groups at the bilayer center. However, this modification unnecessarily complicates the partitioning contribution of each component within the multi-component system. As such, in the present analysis only one strip is used to represent the entire hydrocarbon region. The partitioning of probability distributions for lipid and cholesterol are then carried out based on simple complementarity, where the integrated probability is always equal to one. In other words, the probability of the lipid's hydrocarbon region is reduced such that there is "room" for the cholesterol (see Fig. 2).

3 Results and discussion

There are two sets of parameters that determine the entire SANS curve: In the low-q region, scattering is sensitive to large length-scales, *i.e.* the overall size of the ULV, while the information about bilayer structure is contained in the mid- and high-q regions. Two parameters describe the size distribution function of ULVs (*i.e.* R_m and σ_R), while two others define our bilayer model (*i.e.* A_L and N'_W). In addition, there are two linear parameters corresponding to a multiplicative scaling coefficient and an additive background constant. In total, there are six fitting parameters.

Structural parameters are refined in terms of an iterative model-fitting approach, which result in the bilayer profile. Experimentally obtained scattering curves have been fitted with those which are calculated, in accordance to the previous section. Best fits for particular data sets are shown in Figure 1, while their corresponding 1-D SLD profiles are shown in Figure 3.

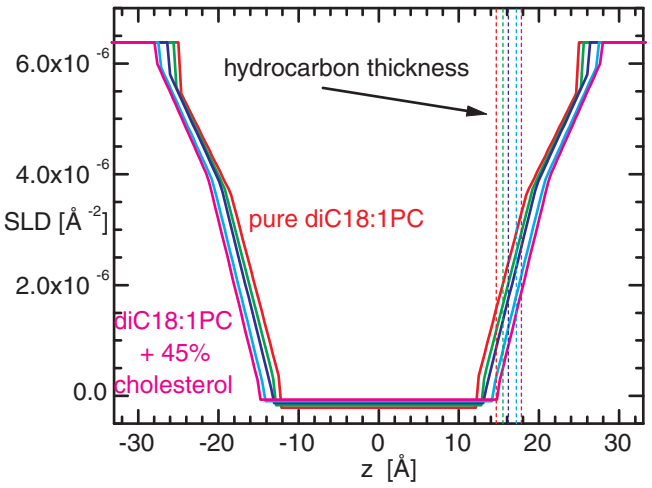

Fig. 3. (Color online) 1-D SLD profiles obtained from best fits to the data. As a function of cholesterol concentration, the overall shape of the profiles remains unchanged, while bilayer thickness increases. The vertical dashed lines demarcate Gibb's dividing surface between the headgroup and hydrocarbon regions.

Figure 3 shows the characteristically large contrast observed between the hydrocarbon region and outside solvent, which gradually decreases within an interfacial region until the boundary between the lipid headgroups and the water is reached. All 1-D SLD profiles show this behaviour, typical of protonated phospholipid bilayers dispersed in D_2O. However, there are also two bilayer properties that are continuously changing as a function of cholesterol content. First, there are increases to the hydrocarbon SLD with increasing amounts of cholesterol —although this change is very small as a result of the cholesterol and the lipid hydrocarbon region having similar SLDs. More importantly, results in Figure 3 show definite increases in bilayer thickness as a function of cholesterol concentration.

This observation is consistent with our fluorescence anisotropy measurements. Values for diC18:1PC ULVs as a function of cholesterol content are shown in Table 2. Increases in anisotropy with the addition of cholesterol are indicative of an increase in the acyl chain order of fluid lipid bilayers [31]. This monotonic increase suggests a concomitant increase in the membrane hydrophobic thickness, since it has been demonstrated elsewhere that these parameters are well correlated [13]. Moreover, our observation that the influence of cholesterol continues to increase over the entire range of cholesterol concentrations used, indicates that the system has not reached its solubility limit.

Table 2 shows the structural parameters extracted from analysis of the SANS data. Because all of the samples were prepared following the same extrusion procedure, it is expected that they have similar size distributions with only small changes induced by the cholesterol [43]. However, there seem to be substantial differences to the ULV mean radius, R_m and polydispersity σ_R of samples containing 38 and 45 mol % cholesterol. They become larger and less uniform with increasing concentration of cholesterol. In addition, there is indication that these two

Table 2. Structural parameters for diC18:1PC ULVs with differing concentration of cholesterol.

cholesterol fraction	0 %	17 %	29 %	38 %	45 %
cholesterol ratio	0	0.20	0.41	0.61	0.82
fluorescence anisotropy	0.097 ± 0.003	0.117 ± 0.003	0.140 ± 0.001	0.164 ± 0.001	0.189 ± 0.002
vesicle radius R_m	312 ± 11	324 ± 16	313 ± 20	344 ± 15	377 ± 20
polydispersity σ_R	97.5 ± 3.5	106 ± 5.2	93.3 ± 5.9	123 ± 5.4	158 ± 8.4
area per unit cell A_{UC}	65.9 ± 1.3	70.8 ± 1.4	76.2 ± 1.8	79.2 ± 2.4	83.9 ± 2.7
total thickness d_{TOT}	49.5 ± 0.7	51.0 ± 0.7	52.3 ± 0.8	54.3 ± 1.1	55.6 ± 1.2
hydrocarbon thickness d_C	14.8 ± 0.3	15.5 ± 0.4	16.2 ± 0.4	17.2 ± 0.6	17.8 ± 0.6
hydration level N'_W	11.0 ± 0.3	12.6 ± 0.3	14.3 ± 0.4	15.4 ± 0.6	16.9 ± 0.8

samples do not only contain ULVs. Scattering curves (Fig. 1) corresponding to these samples show small, broad peaks at $q \sim 0.08\,\text{Å}^{-1}$. Such peaks suggest the presence of pauci-lamellar vesicles (PLVs) [30] made up of a few bilayers, instead of a single bilayer characteristic of ULVs. To account for pauci-lamellarity, we have included an additional Gaussian function in equation (1), which improved the quality of the fits considerably. Nevertheless, the fitting results obtained from these samples should be clearly distinguished from the others.

The second set of parameters shown in Table 2 are associated with the bilayer, itself. A_{UC} is the lateral area of a unit cell (consisting of a lipid and a fraction of cholesterol), while the thicknesses d_{TOT} and d_C correspond to the total bilayer thickness and the hydrocarbon chain thickness, respectively. Finally, N'_W gives the number of water molecules located in the headgroup region. The errors shown in Table 2 correspond to the statistical uncertainties obtained from each particular fitting procedure. It should be noted, however, that there is also a systematic error contributing to all of the fitting results. One of the biggest sources of this error is the volumetric value for the lipid headgroup, V_H, which has been reported to be between 319 and 331 Å^3 [44,40,45]. Nevertheless, this 3% variation affected our final results by $\sim 1\%$ only.

Comparison of results from pure diC18:1PC bilayers with those in the literature [42,46,47], reveals rather large differences. It should be pointed out, however, that in the literature there are also inconsistencies between X-ray and neutron scattering data, especially when it comes to lipid area [28,36,48]. So, why is the area per lipid as obtained from SANS smaller than that from SAXS? In both cases, the area is calculated from the thickness of the hydrocarbon region and well-known volumetric information [49]. On the other hand, for the two techniques this thickness is determined using different models. The best defined structural feature from electron density profiles are the peaks corresponding to lipid phosphate groups, hence their separation across a bilayer d_{HH}. The thickness of the hydrocarbon region is then calculated by assuming that the distance from the phosphate to the interface of the hydrocarbon region (d_{H1}) is known (*e.g.* $d_{H1} = 4.95\,\text{Å}$ was used in [42]). It is typically adapted from the well determined structural results of gel phase bilayers, where the headgroup properties are believed to be the same [46]. Nevertheless, the implications of d_{H1} on the obtained bilayer structure have been previously investigated in detail by Klauda *et al.* [50]. In the case of SANS, the high contrast between the protonated lipid and the deuterated water defines the overall thickness of the bilayer. From that, the hydrocarbon region thickness is obtained using the thickness of the polar headgroup region (d_P). The commonly used value of $d_P = 10\,\text{Å}$ is usually obtained from simulations [29], and provides the best fits to the data.

As the experimentally obtained parameters (*i.e.* d_{HH} and/or d_{TOT}) correspond to different bilayer features, it is impossible to compare them directly. Instead, models —based on information from other techniques *e.g.*, simulations— are used to extract the remaining structural parameters. Unfortunately, results based on this approach may be biased by the numerical results from simulations. On the other hand, simultaneous analysis of the SAXS and SANS data eliminates this dependence if it only employs the functional form of a probability distribution (obtained from simulations) and not its numerical values (*e.g.*, distances between probability distributions). Even though we cannot compare the results, on an absolute scale, from the two different approaches, relative changes are readily detectable [28]. Our present results are shown in Figure 4. All parameters increase monotonically with cholesterol content, and each set of parameters falls nicely on a curve having a small quadratic dependence. This dependence agrees well with our expectations, which is based on the fluorescence anisotropy data (see Tab. 2).

Increases to the bilayer thickness (d_{TOT} and d_C) coincide nicely with previous X-ray diffraction studies [51]. For a 0.5 cholesterol:diC18:1PC mixture, Gandhavadi *et al.* [51] observed an increase in the headgroup peak separation d_{HH} of $\sim 2.5 \pm 1.1\,\text{Å}$. Although we have not studied a similar cholesterol concentration, we can estimate a corresponding change in d_{TOT} using the quadratic function which we used to fit our experimental data. From it, we obtain a $\Delta d_{TOT} \sim 4 \pm 1\,\text{Å}$, which is in close agreement with the experimental value of Gandhavadi *et al.* On the other hand, our observation of an increased bilayer thickness is in contrast with the findings reported by Gallová, *et al.* [21]. They observed no significant change in the thickness of diC18:1PC bilayers, even after the addition of up to 40 mol % cholesterol. In their case, bilayer thickness was determined from SANS data which was evaluated using the small-angle Kratky-Porod approximation and assuming a membrane with a uniform SLD. However, this

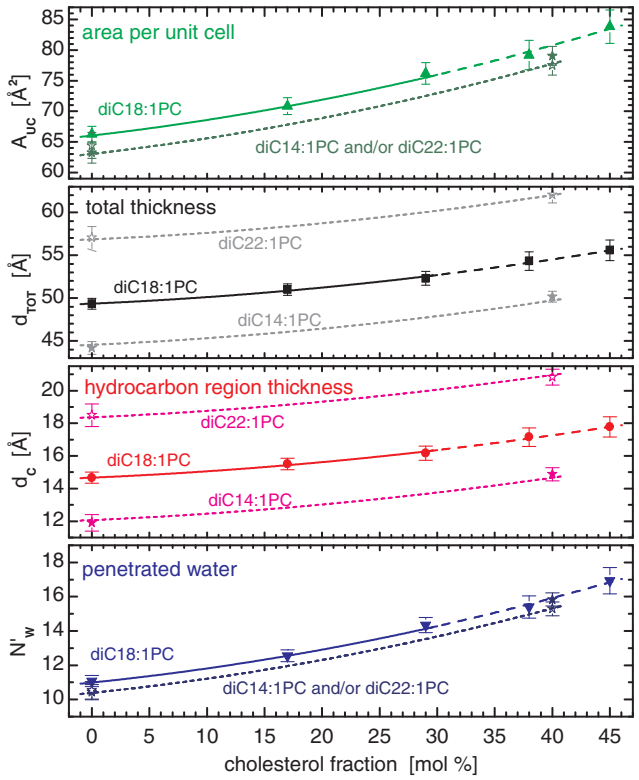

Fig. 4. (Color online) Bilayer parameters plotted as a function of cholesterol concentration for three monounsaturated phospholipids with different chain length. All of the parameters exhibit a quadratic dependence as a function of cholesterol concentration. Quadratic functions were fitted to diC18:1PC (solid lines) and then shifted to serve as guide-lines in case of the two other lipid systems (dotted lines). Dashed lines correspond to the range in which the results may have been affected by pauci-lamellar vesicles.

analysis may be less than accurate, as the SLD changes in the headgroup region. In our model this "smooth" change in the SLD is taken into account by the number of water molecules, N'_W, assigned inside the headgroup region. As is shown in Figure 4, N'_W also increases quadratically with increasing cholesterol concentration.

This increase in hydration is not surprising and is in agreement with numerous studies [14–18]. Previous findings show that the addition of cholesterol results in the following two changes to the bilayer: a) a thickening of the hydrocarbon region, and b) increased hydration of the lipid headgroup. The former is indirectly supported by our fluorescence anisotropy measurements as well as, from our analysis of the SANS data. Furthermore, our results show that the more hydrated headroup can be attributed to cholesterol's effect as a spacer molecule. In other words, more water penetrates into the headgroup region because of an increased separation between lipid headgroups. To our knowledge, this is the first direct observation of cholesterol-induced increases to the hydration of the lipid headgroup region.

Table 3. Structural parameters of diC14:1PC ULVs for two different concentrations of cholesterol.

cholesterol fraction	0%	40%
cholesterol ratio	0	0.67
vesicle radius R_m	302 ± 27	329 ± 20
polydispersity σ_R	103 ± 9.0	98.3 ± 6.3
area per unit cell A_{UC}	63.1 ± 3.5	79.0 ± 3.1
total thickness d_{TOT}	44.1 ± 1.5	50.2 ± 1.3
hydrocarbon thickness d_C	11.9 ± 0.5	14.9 ± 0.4
hydration level N'_W	10.4 ± 0.9	15.8 ± 0.8

Table 4. Structural parameters of diC22:1PC ULVs for two different concentrations of cholesterol.

cholesterol fraction	0%	40%
cholesterol ratio	0	0.67
vesicle radius R_m	285 ± 17	327 ± 31
polydispersity σ_R	80.7 ± 5.1	99.8 ± 9.6
area per unit cell A_{UC}	64.5 ± 4.2	77.7 ± 3.3
total thickness d_{TOT}	57.1 ± 2.6	62.1 ± 1.9
hydrocarbon thickness d_C	18.5 ± 0.7	20.8 ± 0.5
hydration level N'_W	10.6 ± 1.0	15.3 ± 0.8

It was previously shown that cholesterol can either increase or decrease bilayer thickness, depending on the phospholipid's thermodynamic state, acyl chain length and degree of unsaturation [20–23]. For example, bilayer thickening was reported for fully hydrated bilayers with saturated acyl chains ranging in length from 12 to 18 carbons [20]. To address this issue in monounsaturated lipids, we have investigated cholesterol's influence on bilayers made of lipids with differing chain-lengths. Our results for diC14:1PC and diC22:1PC are shown in Tables 3 and 4, respectively.

We compare these results to those obtained for diC18:1PC bilayers in Figure 4. Plots of the pure-lipid area are somewhat surprising. However, it was recently suggested elsewhere [52], that lipids with monounsaturated acyl chains exhibit a maximum lipid area when $n = 18$. Karlovská *et al.* [52] rationalize this in terms of the interplay between the van der Waals attraction and entropic repulsion forces, which possibly depend on the position of the double bond along the acyl chain —the position of double bonds in diC14:1PC and diC18:1PC is 9-*cis*, and in diC22:1PC bilayers it is found at the 13-*cis* position.

Another justification for the present results can be made on the consistency of the various parameters obtained from the same structural model (see Eq. (9)). As such, the two thickness parameters (*i.e.* d_{TOT} and d_C) behave in accordance to general expectations, where the longest lipid produces the thickest bilayer and vice versa. Further, the hydration level is, within experimental error, the same for all three lipids. This is consistent with and confirms the expectation that the structural properties of fully hydrated lipid headgroups depend only on their functional groups (*e.g.* PC) [28]. In our case, all of

the lipids examined were comprised of the same, phosphatidylcholine headgroup.

The influence of cholesterol on ULV bilayers made of short- and long-chain lipids (Fig. 4) reveals an interesting result. Despite having only two data points, the striking similarities to previously determined dependencies prompted us to use the same quadratic functions, only shifted vertically (dotted lines in Fig. 4). These lines are suggestive of the same influence of cholesterol on the three different lipids examined. This result is surprising, especially, in the case of the diC22:1PC lipid whose hydrocarbon region (18.5 Å) seems to be more extended than the overall length of a cholesterol molecule (~ 17 Å [21]).

The widely accepted model of lipid-cholesterol interactions, is that cholesterol affects the membrane structure in two ways [7, 9–18, 20–23]. Firstly, due to its rigid structure cholesterol increases lipid acyl chain order. For a highly flexible fluid phase lipid molecule, such an interaction results in an increased bilayer thickness. Secondly, it is believed that the rigid hydrophobic molecule of cholesterol determines the thickness of the hydrocarbon chain region. Therefore, in the case of long-chain lipids, cholesterol is expected to decrease the thickness of the hydrocarbon chain region. However, our results suggest otherwise. We observe a thickening of the hydrocarbon chain region, even for diC22:1PC bilayers, implying that cholesterol prefers to further order the lipid's hydrocarbon chain over the possibility of rectifying the hydrocarbon chain mismatch.

Although this is a somewhat unexpected result, it can be related to observations reported in the literature. Cholesterol promotes the formation of a liquid-ordered phase, often referred-to as a "raft", which may provide a specialized environment for protein function. Some membrane proteins show activity only in the presence of specific, non-annular lipids, while another probably important factor is the thickness of the hydrocarbon core of the bilayer [53]. For example, the effect of lipid acyl chain length on the activity of Na,K-ATPase was investigated in the presence and absence of 40 mol % of cholesterol [5]. It was shown that the maximum specific activity of the enzyme was reached in diC22:1PC bilayer, while the addition of cholesterol shifted the Na,K-ATPase maximum activity to the diC18:1PC bilayer. This, in agreement with our results, suggests that 40 mol % cholesterol increases the thickness of diC18:1PC bilayer such that it is comparable to the thickness of pure diC22:1PC bilayer. However, the discussed effect of cholesterol on Na,K-ATPase activity may not be entirely the result of increased hydrophobic bilayer thickness, and may be the result of some additional mechanism [19]. Nevertheless, the present results may be used to address this question and can aid in reaching a general understanding of cholesterol-lipid-protein interactions taking place in a biological membrane.

4 Conclusions

We have investigated the influence of cholesterol on membranes made from varying length di-monounsaturated acyl chain (*i.e.* diCn:1PC, $n = 14, 18, 22$) phosphatidylcholines. From SANS measurements of ULV bilayers containing various amounts of cholesterol we were able to determine the various bilayer structural parameters namely, lateral area, total bilayer thickness, hydrocarbon chain thickness and headgroup hydration. For all three systems increasing cholesterol content resulted in a monotonic increase of the various bilayer parameters. While these results were expected in the case of diC14:1PC and diC18:1PC bilayers, this was not the case for the long-chain diC22:1PC bilayers. As the hydrocarbon region of this lipid was found to be longer than cholesterol itself, it was assumed that the addition of cholesterol would result in a thinner bilayer. The observed increase in bilayer thickness suggests that the hydrocarbon ordering effect of cholesterol dominates over its ability to reduce the hydrophobic mismatch between itself and the long-chain lipid.

The authors thank Pavol Balgavý and John Nagle for their valuable comments and their critical reading of the manuscript. J.P. thanks Rumiana Dimova for valuable discussions and for access to her lab, where some of this work was performed. We acknowledge the support of the National Institute of Standards and Technology, U.S. Department of Commerce, in providing the neutron research facilities used in this work. N.K. and J.P. were supported through the Visiting Fellows program of the Natural Sciences and Engineering Research Council of Canada.

References

1. F.W. Pfrieger, Biochim. Biophys. Acta **1610**, 271 (2003).
2. J.R. Silvius, Biochim. Biophys. Acta **1610**, 174 (2003).
3. A. Filippov, G. Oradd, G. Lindblom, Biophys. J. **84**, 3079 (2003).
4. D. Needham, T.J. McIntosh, E. Evans, Biochemistry **27**, 4668 (1988).
5. F. Cornelius, Biochemistry **40**, 8842 (2001).
6. H. Ohvo-Rekilä, B. Ramstedt, P. Leppimäki, J.P. Slotte, Prog. Lipid Res. **41**, 66 (2002).
7. A.G. Lee, Biochim. Biophys. Acta **1612**, 1 (2003).
8. R.S. Lam, A.R. Shaw, M. Duszyk, Biochim. Biophys. Acta **1667**, 241 (2004).
9. M.R. Vist, J.H. Davis, Biochemistry **29**, 451 (1990).
10. T.P.W. McMullen, R.N.A.H. Lewis, R.N. McElhaney, Biochemistry **32**, 516 (1993).
11. P.L.-G. Chong, A.R. Cossins, Biochim. Biophys. Acta **772**, 197 (1984).
12. P.L. Yeagle, Biochim. Biophys. Acta **815**, 33 (1985).
13. F.A. Nezil, M. Bloom, Biophys. J. **61**, 1176 (1992).
14. P.L. Yeagle, W.C. Hutton, C.-H. Huang, R.B. Martin, Biochemistry **16**, 4344 (1977).
15. M.F. Brown, J. Seelig, Biochemistry **17**, 381 (1978).
16. W.K. Subczynski, A. Wisniewska, J.-J. Yin, J.S. Hyde, A. Kusumi, Biochemistry **33**, 7670 (1994).
17. D. Marsh, Eur. Biophys. J. **31**, 559 (2002).
18. C. Ho, S.J. Slater, C.D. Stubbs, Biochemistry **34**, 6188 (1995).
19. F. Cornelius, N. Turner, H.R. Christensen, Biochemistry **42**, 8541 (2003).

20. T.J. McIntosh, Biochim. Biophys. Acta **513**, 43 (1978).
21. J. Gallová, D. Uhríková, A.H. Islamov, A.I. Kuklin, P. Balgavý, Gen. Physiol. Biophys. **23**, 113 (2004).
22. J. Gallová, D. Uhríková, M. Hanulová, J. Teixeira, P. Balgavý, Colloids Surf. B **38**, 11 (2004).
23. M. Pasenkiewicz-Gierula, W.K. Subczynski, A. Kusumi, Biochimie **73**, 1311 (1991).
24. J. Huang, J.T. Buboltz, G.W. Feigenson, Biochim. Biophys. Acta **1417**, 89 (1999).
25. M.R. Brzustowicz, V. Cherezov, M. Zerouga, M. Caffrey, W. Stillwell, S.R. Wassall, Biochemistry **41**, 12509 (2002).
26. A. Parker, K. Miles, K.H. Cheng, J. Huang, Biophys. J. **86**, 1532 (2004).
27. T.A. Harroun, J. Katsaras, S.R. Wassall, Biochemistry **45**, 1227 (2006).
28. J.F. Nagle, S. Tristram-Nagle, Biochim. Biophys. Acta **1469**, 159 (2000).
29. N. Kučerka, J.F. Nagle, S.E. Feller, P. Balgavý, Phys. Rev. E **69**, 051903 (2004).
30. N. Kučerka, J. Pencer, J.N. Sachs, J.F. Nagle, J. Katsaras, Langmuir **23**, 1292 (2007).
31. B. Lentz, Chem. Phys. Lipids **64**, 99 (1993).
32. D.C. Mitchell, B.J. Litman, Biophys. J. **75**, 896 (1998).
33. C.J. Glinka, J.G. Barker, B. Hammouda, S. Krueger, J.J. Moyer, W.J. Orts, J. Appl. Cryst. **31**, 430 (1998).
34. S.R. Kline, J. Appl. Cryst. **39**, 895 (2006).
35. J. Pencer, S. Krueger, C. Adams, J. Katsaras, J. Appl. Cryst. **39**, 293 (2006).
36. P. Balgavý, M. Dubničková, N. Kučerka, M.A. Kiselev, S.P. Yaradaikin, D. Uhríková, Biochim. Biophys. Acta **1512**, 40 (2001).
37. P.C. Mason, B.D. Gaulin, R.M. Epand, G.D. Wignnall, J.S. Lin, Phys. Rev. E **59**, 3361 (1999).
38. J. Pencer, F.R. Hallett, Phys. Rev. E **61**, 3003 (2000).
39. N. Kučerka, M.A. Kiselev, P. Balgavý, Eur. Biophys J. **33**, 328 (2004).
40. D. Uhríková, P. Rybár, T. Hianik, P. Balgavý, Chem. Phys. Lipids **145**, 97 (2007).
41. A. Greenwood, S. Tristram-Nagle, J.F. Nagle, Chem. Phys. Lipids **143**, 1 (2006).
42. N. Kučerka, S. Tristram-Nagle, J.F. Nagle, J. Membr. Biol. **208**, 193 (2005).
43. P. Patty, B.J. Frisken, Biophys. J. **85**, 996 (2003).
44. W.-J. Sun, R.M. Suter, M.A. Knewtson, C.R. Worthington, S. Tristram-Nagle, R. Zhang, J.F. Nagle, Phys. Rev. E **49**, 4665 (1994).
45. S. Tristram-Nagle, Y. Liu, J. Legleiter, J.F. Nagle, Biophys. J. **83**, 3324 (2002).
46. S. Tristram-Nagle, H.I. Petrache, J.F. Nagle, Biophys. J. **75**, 917 (1998).
47. Y. Liu, J.F. Nagle, Phys. Rev. E **69**, 040901 (2004).
48. N. Kučerka, Y. Liu, N. Chu, H.I. Petrache, S. Tristram-Nagle, J.F. Nagle, Biophys. J. **88**, 2626 (2005).
49. J.F. Nagle, R. Zhang, S. Tristram-Nagle, W. Sun, H.I. Petrache, R.M. Suter, Biophys. J. **70**, 1419 (1996).
50. J.B. Klauda, N. Kučerka, B.R. Brooks, R.W. Pastor, J.F. Nagle, Biophys. J. **90**, 2796 (2006).
51. M. Gandhavadi, D. Allende, A. Vidal, S.A. Simon, T.J. McIntosh, Biophys. J. **82**, 1469 (2002).
52. J. Karlovská, D. Uhríková, N. Kučerka, J. Teixeira, F. Devínsky, I. Lacko, P. Balgavý, Biophys. Chem. **119**, 69 (2006).
53. A.G. Lee, Biochim. Biophys. Acta **1666**, 62 (2004).